Journal of Power Sources 249 (2014) 163–171

Contents lists available at ScienceDirect

Journal of Power Sources

journal homepage: www.elsevier.com/locate/jpowsour

Comparison of the anodic behavior of aluminum current collectors in imide-based ionic liquids and consequences on the stability of high voltage supercapacitors

Ruben-Simon Kühnel, Andrea Balducci*

University of Muenster, MEET Battery Research Center and Institute of Physical Chemistry, Corrensstr. 28/30, 48149 Münster, Germany

HIGHLIGHTS

- Comparison of the anodic behavior of Al current collectors in two ionic liquids.
- Good passivation of Al in $PYR_{14}TFSI$.
- Stability of Al in $PYR_{14}FSI$ depends on the purity of the ionic liquid.
- The different Al stability affects the behavior of supercapacitors during float tests.

ARTICLE INFO

Article history:
Received 9 August 2013
Received in revised form
30 September 2013
Accepted 10 October 2013
Available online 25 October 2013

Keywords:
Aluminum
Corrosion
Passivation
Ionic liquid
FSI
TFSI
EDLC

ABSTRACT

In this work, the influence of two common ionic liquid (IL) anions on the anodic stability of Al current collectors was studied. Namely, the Al corrosion/passivation process in *N*-butyl-*N*-methylpyrrolidinium bis(trifluoromethanesulfonyl)imide ($PYR_{14}TFSI$) is compared to the one in *N*-butyl-*N*-methylpyrrolidinium bis(fluorosulfonyl)imide ($PYR_{14}FSI$). It is shown, that Al slowly corrodes in $PYR_{14}FSI$, while it is much better passivated in $PYR_{14}TFSI$, although the ionic liquids were prepared in the same way. Float tests were carried out to illustrate the consequences of these different anodic stabilities of Al on the cycling stability of supercapacitors. Interestingly, when the chloride content of $PYR_{14}FSI$ was <1 ppm, Al electrodes were also pretty stable in this IL, and a similar cycling stability during float tests than for $PYR_{14}TFSI$ could be obtained.

1. Introduction

Ionic liquids are an emerging class of electrolytes for electrochemical devices like electrochemical double-layer capacitors (EDLCs; also called supercapacitors) and lithium-ion batteries (LIBs) due to their broad electrochemical windows, moderate to high conductivities and high intrinsic safety due to very low vapor pressures [1]. Among the various cation–anion combinations that have been investigated, ionic liquids with imidazolium- or pyrrolidinium-based cations and bis[(perfluoroalkyl)sulfonyl]imide anions have attracted the attention of the LIB and supercapacitor community due to their remarkable wide electrochemical stability windows and acceptable to good conductivities. Successful application of such ILs has been shown in combination with many common LIB and supercapacitor electrode materials, *e.g.* graphite [2], lithium titanate (LTO) [3], lithium cobalt oxide (LCO) [4], lithium iron phosphate (LFP) [5], lithium nickel manganese cobalt oxide (NMC) [6] and activated carbon (AC) [7–11].

Among the bis[(perfluoroalkyl)sulfonyl]imide anions investigated so far, the anions bis(trifluoromethanesulfonyl)imide ($TFSI^-$) and bis(fluorosulfonyl)imide (FSI^-) have been the most investigated. Typically, FSI-based ILs have lower viscosities (due to the smaller size of the anion) and thus higher conductivities than the TFSI-based ones [4]. On the other hand, TFSI-based ILs display higher thermal and electrochemical stability compared to the FSI-based ones [12].

In view of the development of innovative electrolytes, not only transport properties and electrochemical stabilities have to be

* Corresponding author.
E-mail address: andrea.balducci@uni-muenster.de (A. Balducci).

0378-7753/$ – see front matter © 2013 Elsevier B.V. All rights reserved.
http://dx.doi.org/10.1016/j.jpowsour.2013.10.072

taken into account, but also the compatibility of the electrolyte with inactive components of the device, *e.g.* current collectors, has to be carefully considered. The current collector material of choice for LIB cathodes and both negative and positive supercapacitor electrodes is aluminum (Al). Al has a variety of advantages: it is light, easy to process, relatively inexpensive and has a good electrical conductivity. Nevertheless, Al as a base metal is thermodynamically not stable at high potentials reached in the cathode of LIBs or the positive electrode of high voltage supercapacitors. Hence, the surface of the Al has to be passivated by reaction with electrolyte components to prevent its dissolution. In the last years, the anodic behavior of Al in different ionic liquids containing $TFSI^-$ and FSI^- has been studied [13–18]. In the case of ILs containing $TFSI^-$, several works showed that under polarization the Al is much more stable in this type of ILs than in solutions composed of organic solvent and $TFSI^-$ containing salt, *e.g.* PC–LiTFSI [17]. There is evidence, that *e.g.* $TFSI^-$ anions attack the Al surface under polarization leading to the formation of Al-TFSI species. Such species are soluble in polar molecular solvents, *e.g.* PC, and therefore they cannot form a protective layer on the Al surface, which is consequently subject to a corrosion process [19]. To the contrary, Al-TFSI species are thought to be poorly soluble in common ILs for electrochemical applications, *e.g.* $PYR_{14}TFSI$, and such poor solubility makes the formation of a protective layer on the Al surface possible [14,17,18]. In the case of FSI-based ILs the anodic behavior of Al seems to be different, as it was recently shown that in the electrolyte $PYR_{13}FSI$–LiTFSI progressing Al dissolution takes place [16]. Considering the results of these studies, TFSI- and FSI-based ILs seem therefore to display a different behavior regarding the Al corrosion.

In the past several TFSI- and FSI-based ILs have been widely investigated as electrolyte for EDLCs [7–11]. The results of these studies indicate that both types of ILs are promising candidates for the realization of high voltage EDLCs. Nevertheless, to the best of our knowledge, a comparative study about the influence of Al corrosion on the behavior of EDLCs containing these ILs has never been carried out. Taking into account the different ability to prevent the Al corrosion mentioned above, such study could be extremely useful to further understand the advantages and limits related to the use of these ILs in EDLCs.

In this manuscript, we investigate the anodic behavior of Al in the two ILs *N*-butyl-*N*-methylpyrrolidinium bis(trifluoromethane sulfonyl)imide ($PYR_{14}TFSI$) and *N*-butyl-*N*-methylpyrrolidinium bis(fluorosulfonyl)imide ($PYR_{14}FSI$). Initially, the conductivity, viscosity and electrochemical stability of the two considered ILs are compared. Afterward, an electrochemical characterization of the corrosion/passivation behavior of Al current collectors under polarization in $PYR_{14}TFSI$ and $PYR_{14}FSI$ is presented. In the third part, the consequence of this behavior on the performance of high voltage EDLCs is considered. Finally, preliminary results on the influence of the chloride content of $PYR_{14}FSI$ on the stability of EDLCs during float tests are presented. Furthermore, cyclic voltammetry is also carried out with a $PYR_{14}FSI$ electrolyte with very low chloride content and the results are compared to the ones obtained for $PYR_{14}FSI$ with a higher level of chloride impurities.

2. Experimental

2.1. Electrolyte preparation

$PYR_{14}TFSI$ and $PYR_{14}FSI$ were synthesized similar to reference [20], using a bromide route. In the following, a shortened description of the synthesis is given. In the first step, *N*-butyl-*N*-methylpyrrolidinium bromide ($PYR_{14}Br$) was synthesized by alkylation of *N*-methylpyrrolidin with 1-bromobutane in ethyl acetate at 35 °C for 48 h. In the second step, $PYR_{14}Br$ was reacted with a small excess (3 wt%) of LiTFSI (3 M, battery grade) or K-FSI (Dai-Ichi Kogyo Seiyaku) in deionized H_2O for min. 1 h at room temperature to obtain $PYR_{14}TFSI$ or $PYR_{14}FSI$, respectively. The ionic liquids were then washed with deionized H_2O 5 times to remove the alkali halides and excess LiTFSI or K-FSI, respectively. The ILs were then purified with alumina and charcoal in ethyl acetate and finally dried stepwise with an oil pump (<0.01 mbar) and a turbomolecular pump ($<1 \times 10^{-5}$ mbar) while heating up to 60 ($PYR_{14}FSI$) or 90 °C ($PYR_{14}TFSI$), consecutively. The water contents of the dried ionic liquids were <10 ppm as measured by Karl-Fischer titration, respectively. A second batch of $PYR_{14}FSI$ with lower chloride content was prepared by more carefully washing the IL with deionized H_2O. The chloride contents of both $PYR_{14}FSI$ batches were measured via ion chromatography and found to be >2 ppm for the first batch and <1 ppm for the more carefully prepared second batch.

2.2. Physicochemical characterization

The conductivity of the ionic liquids was measured in a 2-electrode configuration by impedance spectroscopy using a sealed glass cell with two platinum electrodes. The measurements were carried out with a Solartron model 1287A potentiostat coupled with a Solartron model 1260A frequency response analyzer controlled by Corrware software. The cell was placed in a climatic chamber (MK53, Binder) set to 20 °C.

The viscosity of the ionic liquids was measured with an Anton-Paar Physica MCR 301 rheometer in cone-plate configuration at 20 °C.

2.3. Electrochemical characterization

To test the anodic behavior of aluminum in the investigated ionic liquids, electrochemical tests were carried out in 3-electrode Swagelok cells connected to a Bio-Logic VMP3 controlled by EC-Lab software. As working electrode, discs of 12 mm diameter cut out of aluminum foil (purity of ≥99.85%, thickness of 20 μm, rinsed with ethanol, then vacuum dried) were used. The counter electrode was an activated carbon-based electrode (see below). Li was used as reference electrode. The experiments were carried out at 20 °C in climatic chambers.

2.3.1. Chronoamperometry

Initially, the potential of the working electrode was linearly swept from open circuit potential (OCP) to 5 V vs. Li with a scan rate of 1 mV s^{-1}. The potential was then hold for 12 h at 5 V vs. Li and the current was continuously recorded. In the following, all potentials are referred to the lithium reference. This experiment was carried out with $PYR_{14}TFSI$ and $PYR_{14}FSI$ with a chloride content of >2 ppm as electrolyte, respectively.

2.3.2. Cyclic voltammetry

Starting from OCP, the potential was scanned to 5 V, the scanning direction was reversed and the potential was scanned down to 3.3 V. The scan rate was fixed to 0.5 mV s^{-1}. A total of 10 cycles was performed for each cell. This experiment was carried out with $PYR_{14}TFSI$ and with two different batches of $PYR_{14}FSI$, with chloride contents of >2 ppm and <1 ppm, as electrolyte, respectively.

2.4. Activated carbon electrode preparation and testing

Activated carbon (Super DLC30, Norit) was used as received. Sodium carboxymethyl cellulose (CMC) was provided by Dow Wolff

Cellulosics (Walocel CRT 2000 PPA 12) with a degree of substitution of 1.2. Carbon black (Super C65, TIMCAL) was used as conducting agent. Composite electrodes coated on etched Al foil were prepared similar to a procedure described elsewhere [21]. The composition of the dried electrodes was 85 wt% activated carbon, 10 wt% Super C65 and 5 wt% of CMC. The electrode mass loading was *ca.* 3 mg cm^{-2}. The electrode area was 1.13 cm^2.

2.4.1. Cyclic voltammetry

The experiments were carried out between 3.3 and 5 V at a scan rate of 0.5 mV s^{-1} in 3-electrode Swagelok cells connected to a Bio-Logic VMP3 controlled by EC-Lab software. As working electrode, the just described activated carbon electrodes were used. The counter electrode was an activated carbon-based pellet electrode with a high mass loading ($\geq$30 mg cm^{-2}). Li was used as reference electrode. The experiments were carried out at 20 °C in a climatic chamber. Impedance spectra were recorded every 100 cycles at 3.3 V in a frequency range between 500 kHz and 10 mHz with an AC amplitude of 5 mV. This experiment was carried out with $PYR_{14}TFSI$ and $PYR_{14}FSI$ with a chloride content of >2 ppm as electrolyte, respectively.

2.4.2. Float tests

Float tests were carried out in 2-electrode configuration using two of the activated carbon electrodes of equal weight. In the beginning, impedance spectra were recorded at OCP in a frequency range between 500 kHz and 10 mHz with an AC amplitude of 5 mV. Afterward, 50 full charge–discharge cycles were carried out up to 3.5 V at a current density of 5 mA cm^{-2} followed by an impedance measurement. The following three steps were repeated 10 times. The cell was charged to 3.5 V and this potential was hold constant for 20 h. After discharging, again 50 full charge–discharge cycles were carried out followed by an impedance measurement. The float tests were carried out at 20 and 60 °C. The impedance measurements were only carried out for the cells tested at 20 °C. This experiment was carried out with $PYR_{14}TFSI$ and $PYR_{14}FSI$ with a chloride content of >2 ppm as electrolyte, respectively. Additionally, the same float test was carried out with the second batch of $PYR_{14}FSI$ with a chloride content of <1 ppm at 20 °C.

2.5. Surface characterization

The morphology of Al electrodes that had been subjected to cyclic voltammetry up to 5 V (after rinsing with dimethyl carbonate (DMC) and drying under vacuum) and of activated carbon electrodes (after removal of the carbon coating with deionized H_2O in an ultrasonic bath and drying under vacuum) that had been subjected to long-term cyclic voltammetry up to 5 V were investigated by scanning electron microscopy (AURIGA, Carl Zeiss). The surface composition of Al electrodes that had been subjected to cyclic voltammetry up to 5 V and of Al electrodes that had been stored for 24 h without polarization in cells similar to the ones used for the CV experiment (after rinsing with dimethyl carbonate (DMC) and drying under vacuum) were investigated by X-ray photoelectron spectroscopy (XPS), respectively. The XPS measurements were performed on an AXIS Ultra DLD (Kratos) using monochromatic Al Kα radiation. The measurements were repeated at three different points. Core level measurements were performed at pass energies of 20 eV. The calibration of the spectra was done with respect to adventitious carbon (285 eV). The spectra were normalized with respect to the intensity of the carbon peak at 285 eV. The samples were transferred from the glove box into the vacuum chamber without any air contact by using an argon filled transfer vial.

3. Results and discussion

3.1. Comparison of the physicochemical properties of $PYR_{14}TFSI$ and $PYR_{14}FSI$

Conductivity, viscosity and electrochemical stability limit values of $PYR_{14}TFSI$ and $PYR_{14}FSI$ at 20 °C are reported in Table 1. $PYR_{14}FSI$ showed a rather high conductivity and low viscosity for an IL of 5.1 mS cm^{-1} and 60 mPa s, respectively, while $PYR_{14}TFSI$ displayed values of 2.2 mS cm^{-1} and 90 mPa s. The values indicated in Table 1 are, for both ILs, in the range of values previously reported in literature [22,23]. Deviations can probably be associated to different levels of impurities like H_2O, halides or residual organic compounds. It was reported that the electrochemical stability windows on platinum exceed 5 V, if a limiting current of 0.1 mA cm^{-2} is considered. These two ILs were already proposed for the use in supercapacitors and due to their high electrochemical stability windows, both of them have been proposed for the realization of EDLCs with operative voltages $\geq$3.5 V [7,24].

3.2. Anodic behavior of aluminum in TFSI- and FSI-based ionic liquids

As mentioned in the introduction, aluminum is the standard current collector for supercapacitors. In order to develop high voltage EDLCs (as those proposed using $PYR_{14}TFSI$ and $PYR_{14}FSI$), the compatibility of the electrolyte with the Al current collector appears extremely important. As a matter of fact, if the electrolyte does not display the ability to prevent the corrosion of the Al current collector, such process will necessarily lead to a decrease of the EDLC's stability over time.

Fig. 1 shows the current response of an aluminum electrode during a 12 h-chronoamperometry experiment at 5 V. As shown, obvious differences between the two investigated ILs can be observed. In $PYR_{14}FSI$, the current increased during the polarization while it was going down in $PYR_{14}TFSI$. The increasing current in the case of the $PYR_{14}FSI$ electrolyte originated from faradic reactions. Two possible processes can be identified: electrolyte decomposition and/or anodic Al dissolution. Considering that the anodic stability of $PYR_{14}FSI$ on Pt exceeds 5 V (Table 1), it can be assumed that most of the current increase was caused by anodic Al dissolution. In contrast, the decreasing current in the case of $PYR_{14}TFSI$ indicates passivation of the Al.

Big differences were also found in the current response observed during cyclic voltammetry experiments (Fig. 2). While in the case of $PYR_{14}FSI$ (Fig. 2B) the current was increasing with cycle number, it was decreasing for $PYR_{14}TFSI$ (Fig. 2A). After 10 cycles, values exceeding 30 μA cm^{-2} were reached for $PYR_{14}FSI$, while the maximum current density dropped down to values below 2 μA cm^{-2} for $PYR_{14}TFSI$. Furthermore, the shape of the CV curves was different. For the TFSI-based IL, the current suddenly dropped when the scan direction was reversed at 5 V; the typical current response when the surface is passivated. In contrast, the CV curves

Table 1
Conductivity, viscosity and electrochemical stability limits of $PYR_{14}TFSI$ and $PYR_{14}FSI$ at 20 °C. The stability limits are based on a cut-off current density of 0.1 mA cm^{-2}.

Electrolyte	Conductivity/ mS cm^{-1}	Viscosity/ mPa s	Cathodic stability limit/V vs. Li/Li^+	Anodic stability limit/V vs. Li/Li^+
$PYR_{14}TFSI$	2.2	90	0.0[a]	5.8[a]
$PYR_{14}FSI$	5.1	60	0.0[b]	5.35[b]

[a] From Ref. [29]; shifted to the Li/Li^+ scale.
[b] From Ref. [22].

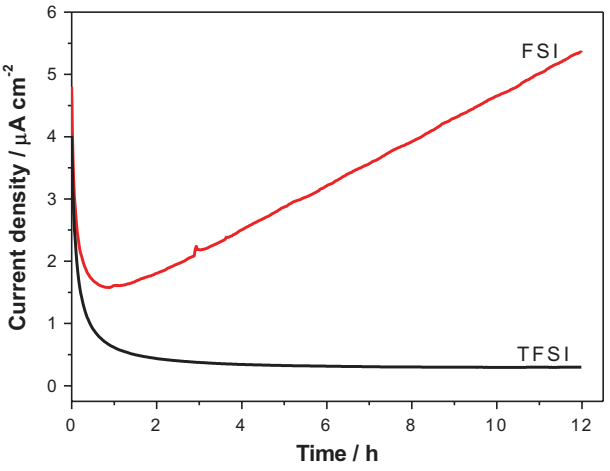

Fig. 1. Chronoamperograms of Al electrodes recorded during polarization at 5 V vs. a lithium reference for 12 h in $PYR_{14}TFSI$ (TFSI) and $PYR_{14}FSI$ (FSI) at 20 °C. An activated carbon-based electrode was used as counter electrode.

using $PYR_{14}FSI$ showed hysteresis (the typical shape indicating the presence of anodic Al dissolution) starting from the second cycle.

After the CV experiment, SEM images of the polarized Al foil electrodes were taken (Fig. 3). The image taken after the CV experiment in $PYR_{14}TFSI$ (Fig. 3A) confirms the good passivation of Al in this IL, while attack of the Al foil is clearly visible in the SEM image taken after the same experiment in $PYR_{14}FSI$ (Fig. 3B). Pitting corrosion spots can be seen on the SEM image. Pitting corrosion usually leads to round corroded spots on the Al surface which can penetrate through the whole thickness of the Al foil over time.

Several works proposed the formation of Al-TFSI compounds in the initial step of the Al corrosion process in TFSI-containing electrolytes [13,18,19,25]. It was also pointed out that the suppression of the corrosion process in TFSI-containing ILs should be related to the low solubility of Al-TFSI species in these ILs. Such a passivation mechanism is somehow similar to the one in PF_6-containing electrolytes, in which the formation of a layer of AlF_3 that is hardly soluble in the electrolyte helps to passivate the Al surface and thus prevents most of the Al corrosion [26].

In the case of FSI-based ILs, the formation of Al-FSI species seems plausible. Taking into account the mild Al corrosion reported above, it can be supposed that either Al-FSI species are slightly soluble in $PYR_{14}FSI$ or that the passivation layer is less resistant to attack from residual halides. This hypothesis is also in line with the recent finding that $PYR_{14}TFSI$ doped with LiFSI also lead to mild Al dissolution under polarization [27].

In our XPS study (Fig. 4), we compared the surface film that formed during the CV experiment up to 5 V with results obtained for Al electrodes that were only kept in identical cells for 24 h without any polarization. All C 1s spectra (Fig. 4A) were rather similar, with the exception that both $PYR_{14}TFSI$ spectra showed an additional peak at *ca.* 293 eV representing the carbons of the CF_3 groups of the $TFSI^-$ anion. The Al 2p spectra (Fig. 4B) showed two peaks, a peak that can be assigned to metallic Al (*ca.* 71.5 eV) and a peak representing Al^{3+} compounds (*ca.* 75 eV). The intensities of the Al^{3+} peaks were relatively higher than the intensities of the Al metal peaks for the Al electrodes that were subjected to cyclic voltammetry compared to the ones of the Al electrodes that were only kept in the electrolyte. This result indicates that the thickness of the films on top of the surface of the Al metal increased during the CV experiment. Unfortunately, the Al 2p spectra of the Al electrodes subjected to cyclic voltammetry showed only one peak except the Al metal peak. However, it is clearly visible in the spectra that the binding energy of this peak shifted to higher binding energies for the electrodes subjected to CV in $PYR_{14}TFSI$ and $PYR_{14}FSI$. Hence, it can be assumed that the new films did not only consist of Al_2O_3 but also of other Al^{3+}-containing compounds like the Al-TFSI/Al-FSI species introduced above. It was shown in literature that the oxide layer plays an important role in the protection of the Al from anodic dissolution in different kinds of electrolytes [26]. But usually the formation of additional insoluble compounds to improve the resistance of Al against corrosion is needed because there are always defects in the oxide layer that allow the attack of Al by anions present in the electrolyte [26]. Therefore, changes in the passivation film can be expected, especially in the case of $PYR_{14}TFSI$, the electrolyte that showed excellent protection of Al. Furthermore, there were differences in the ratios between the N 1s (Fig. 4C) peaks representing the cation (*ca.* 403 eV) and anion (*ca.* 400 eV) of the ILs. Even for the electrodes that were only kept in cells containing the electrolytes without any polarization, there was an excess of N-containing compounds related to the anion ($TFSI^-$ or FSI^-) on the surface. But the ratio of N-containing species found for the Al electrodes after the CV experiment was more on the side of the anions for both ILs than for the Al electrodes that were only kept in the same kind of cells for 24 h. This effect was especially

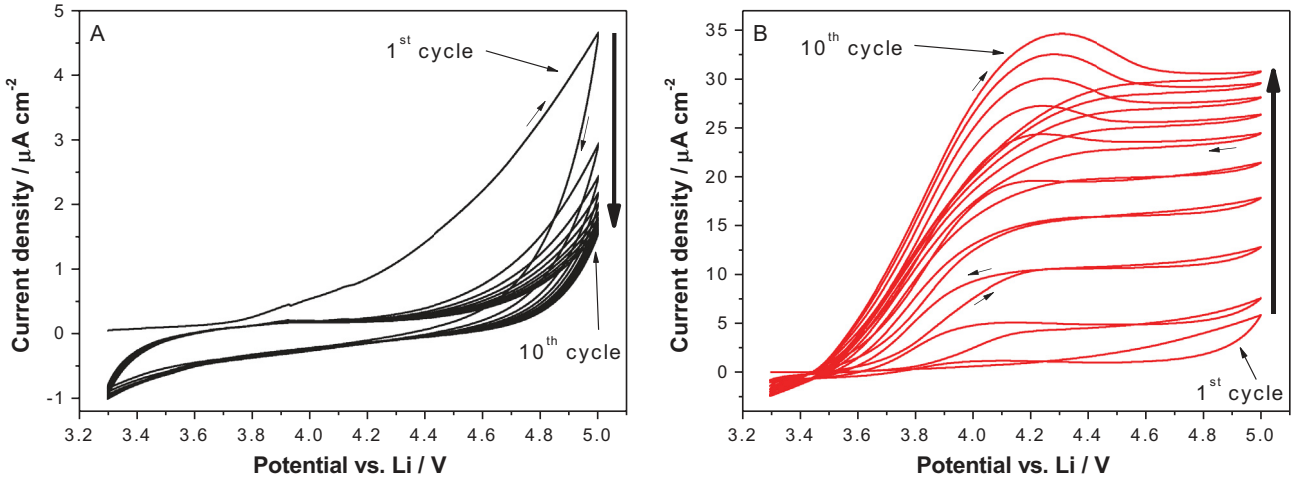

Fig. 2. Cyclic voltammograms of Al electrodes recorded between 3.3 and 5 V vs. a lithium reference in (A) $PYR_{14}TFSI$ and (B) $PYR_{14}FSI$ at 20 °C. Scan rate: 0.5 mV s^{-1}. An activated carbon-based electrode was used as counter electrode.

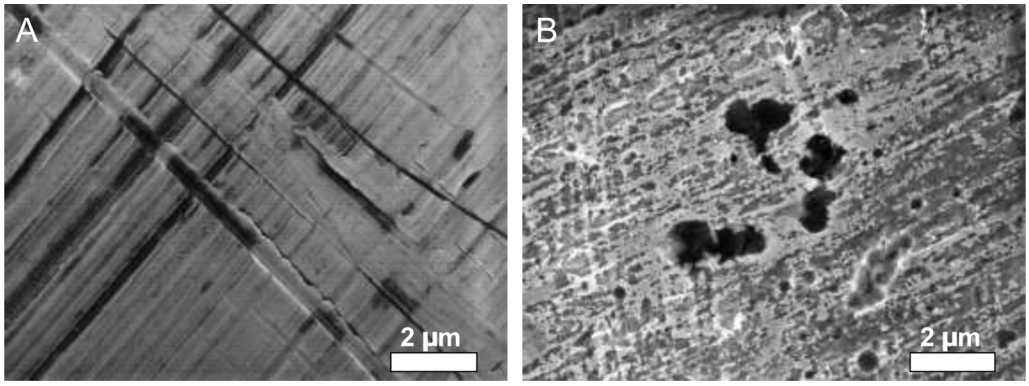

Fig. 3. SEM images of Al electrodes taken after a cyclic voltammetry experiment (see Fig. 2) between 3.3 and 5 V in (A) $PYR_{14}TFSI$ and (B) $PYR_{14}FSI$.

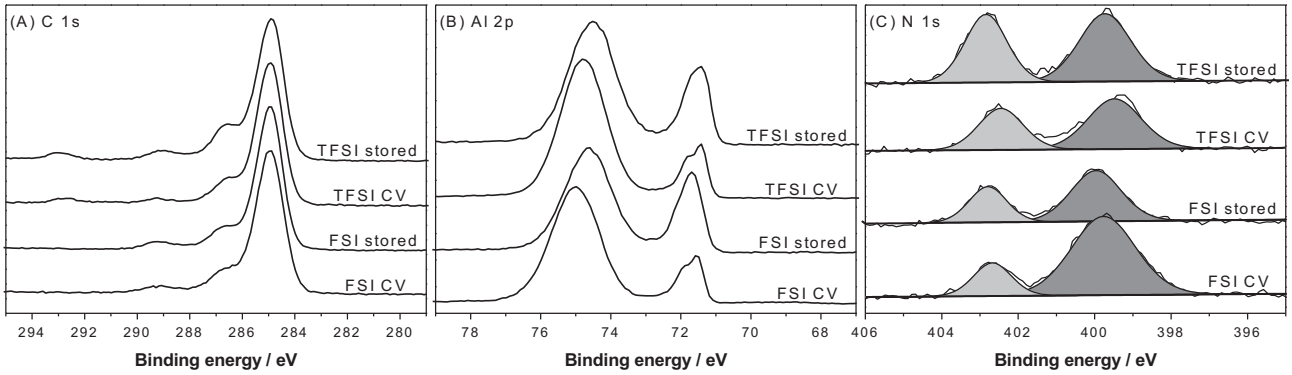

Fig. 4. X-ray photoelectron spectra of Al electrodes after a cyclic voltammetry experiment (see Fig. 2) up to 5 V in $PYR_{14}TFSI$ (TFSI CV) and $PYR_{14}FSI$ (FSI CV) and after storage for 24 h without any polarization in cells similar to the ones used for the CV experiment (TFSI stored, FSI stored).

pronounced for $PYR_{14}FSI$. The question remains whether these increased fractions of $TFSI^-$ and FSI^- originated from Al-TFSI/Al-FSI compounds or whether they were just the result of increased anion adsorption due to polarization of the Al electrodes. Taking into account the shifted Al^{3+} signals and the increased fractions of $TFSI^-/FSI^-$ it is nevertheless plausible to assume the formation of Al-TFSI/Al-FSI species. The bigger relative signal intensity found for FSI^- compared to the smaller one for $TFSI^-$ in the N 1s spectra can also be understood considering the Al corrosion found for $PYR_{14}FSI$. If the corrosion process involves the formation of Al-FSI species, it can be expected that the amount of Al-FSI compounds on the surface is higher than in the case of Al-TFSI compounds for $PYR_{14}TFSI$. Nevertheless, it seems to be necessary to combine XPS with another technique for a future in-depth study of the surface films forming on Al in TFSI or FSI-based ILs. Time-of-flight secondary ion mass spectrometry (ToF-SIMS) was already successfully employed for the study of surface films on Al in $LiPF_6$-based electrolytes [28] and might also be a useful tool to investigate the surface layer forming on Al in FSI- or TFSI-based ILs.

3.3. Consequences of the differences in the anodic stability of Al current collectors on the cycling stability of high voltage EDLCs

Even though the corrosion process we found for $PYR_{14}FSI$ was rather mild, it was shown recently that a Li/LCO coin cell charged up to 4.2 V showed pronounced capacity fading during 50 cycles when the electrolyte was $PYR_{13}FSI$-LiTFSI [16]. Taking into account the fact that in high voltage EDLCs (*e.g.* with an operative voltage of 3.5 V) the positive electrode might reach potentials higher than 4.5 V vs. Li/Li^+, the occurrence of such mild Al corrosion might also affect the behavior of these devices, when FSI-based IL are used.

To the best of our knowledge, the influence of anodic Al dissolution in FSI-based ILs on the behavior of high voltage EDLCs has never been investigated. Therefore, we decided to investigate this point. Moreover, since TFSI and FSI-based ILs have been widely investigated as electrolyte for EDLCs, we also compared the behavior of these two types of IL.

Initially, we carried out CV experiments using an activated carbon working electrode. We chose a slow scan rate of 0.5 mV s^{-1} and a rather high cut-off potential of 5 V to be able to see the effect of Al corrosion in a reasonable number of cycles. An oversized carbon counter electrode was used in order to avoid any influence of the negative electrode on the cycling stability. We then calculated coulombic efficiencies of the charge/discharge process (Fig. 5A). The lower the efficiency, the higher are the contributions of faradic reactions like electrolyte decomposition or Al corrosion to the total charge of a cycle. As shown in Fig. 5A, when $PYR_{14}TFSI$ was used as electrolyte the cycling efficiencies were higher and more stable than in the case of $PYR_{14}FSI$. In the case of $PYR_{14}TFSI$, after an initial activation phase, the cycling efficiency reached a value of 96% which after 700 cycles only slightly decreased to a value of 94.3%. The deviation from full reversibility can mostly be attributed to minor electrolyte decomposition taking place at high potentials close to 5 V. The efficiencies for $PYR_{14}FSI$ were generally lower than for $PYR_{14}TFSI$ due to a higher level of electrolyte decomposition in line with the lower anodic stability of $PYR_{14}FSI$ compared to the one of $PYR_{14}TFSI$ (Table 1). But in contrast to the results obtained for $PYR_{14}TFSI$, the efficiency started to decrease strongly for $PYR_{14}FSI$ after 200 cycles and approached values close to zero after 600

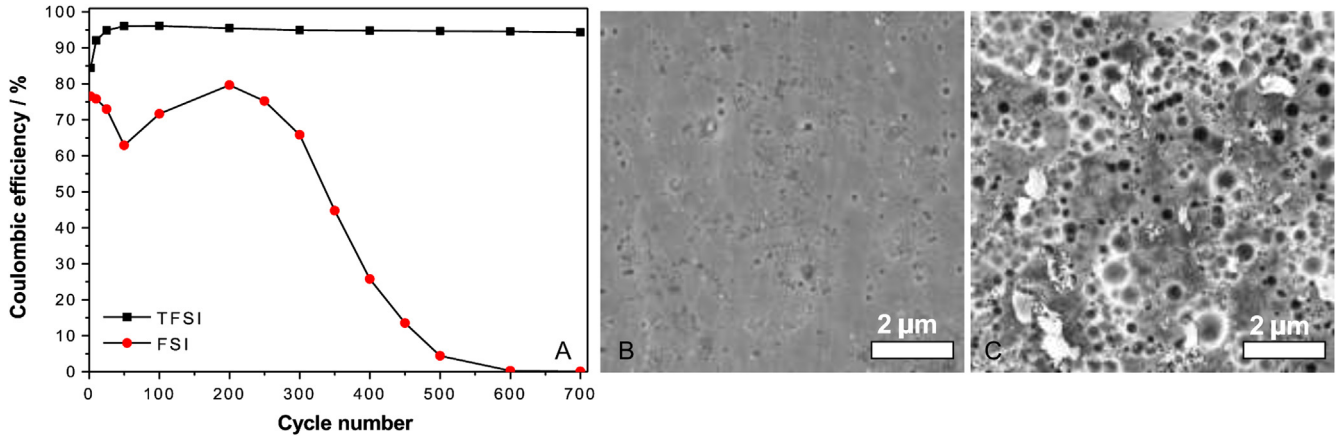

Fig. 5. (A) Coulombic efficiencies calculated from cyclic voltammograms of activated carbon-based electrodes cycled between 3.3 and 5 V vs. a lithium reference in $PYR_{14}TFSI$ (TFSI) and $PYR_{14}FSI$ (FSI), respectively, at 20 °C. Scan rate: 0.5 mV s^{-1}. SEM images of the Al current collectors taken after the CV experiment in (B) $PYR_{14}TFSI$ and (C) $PYR_{14}FSI$. The coating on top of the Al current collector was removed with deionized water in an ultrasonic bath.

cycles. This drop in efficiency was most likely due to progressing Al corrosion which was accelerating over time. Most likely, Al corrosion had only a minor contribution to the irreversibility in the first 200 cycles, because the activated carbon coating on top of the Al foil should delay the occurrence of Al corrosion due to partial blocking of defect sites on the surface of the Al where corrosion preferentially starts. The charge/discharge process became probably almost fully irreversible after a certain number of cycles because the activated carbon particles lost contact to the Al current collector and in course became electrically insulated and thus could not contribute to the double-layer formation anymore.

After the CV experiment, the activated carbon-based coating was removed and SEM images of the current collectors were taken. Fig. 5B and C shows big differences for the two electrolytes. In the case of $PYR_{14}TFSI$ (Fig. 5B), the SEM image shows only rather mild signs of corrosion and additionally some electrolyte decomposition products. In the case of $PYR_{14}FSI$ (Fig. 5C), strong pitting corrosion is clearly visible. There are holes, pitting corrosion spots filled with corrosion products as well as electrolyte decomposition products visible. Most likely, the much longer time spent at high potentials during this long-term CV experiment up to 5 V explains the difference to the milder corrosion than can be seen on the SEM image taken after an Al electrode was subjected to only 10 cycles of CV up to 5 V in $PYR_{14}FSI$ (Fig. 3B). The results obtained for the activated carbon electrodes clearly demonstrated that pronounced pitting corrosion appeared for $PYR_{14}FSI$ while the current collector was much better protected from such corrosion in $PYR_{14}TFSI$. The impedance spectra (Fig. 6) taken during the long-term CV experiment also showed pronounced differences for the two electrolytes. In the case of $PYR_{14}TFSI$ (Fig. 6A), the impedance was generally much more stable and the appearance of the semi-circle was most likely related to the formation of electrolyte decomposition products in the pores of the AC-based electrode. The magnification shows that the high frequency resistance, which is related to the conductivity of the electrolyte, practically did not change after the first 100 cycles, indicating that electrolyte decomposition was not very pronounced. In the case of $PYR_{14}FSI$ (Fig. 6B), the change in impedance during cycling was much more dramatic. The high frequency resistance continuously increased over cycling indicating pronounced electrolyte decomposition. After 100 cycles, a first semi-circle, significantly bigger than in the case of $PYR_{14}TFSI$, had appeared that is probably related to electrolyte decomposition products in the pores of the AC-based electrode. After 300 cycles, a second semi-circle had appeared, while at the same time the

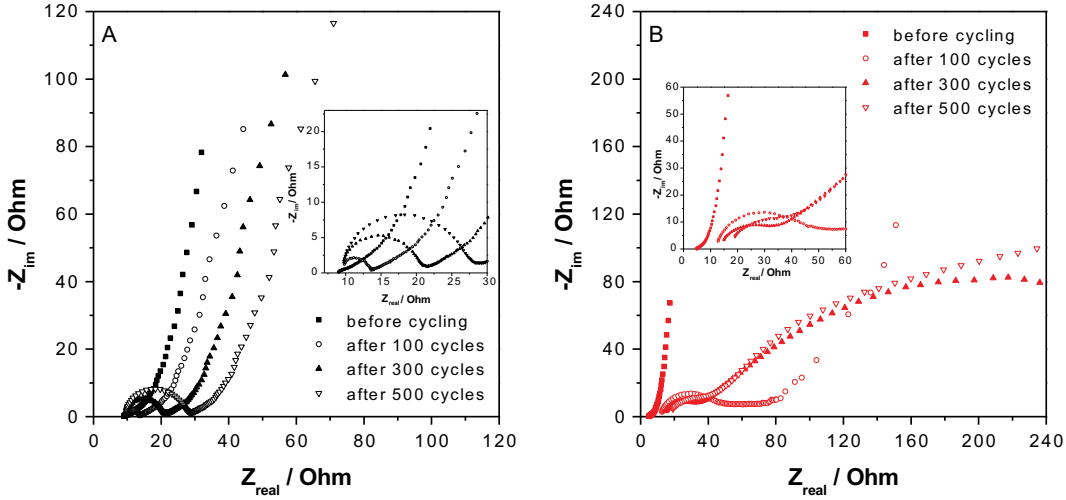

Fig. 6. Evolution of the impedance of activated carbon-based electrodes subjected to cyclic voltammetry (see Fig. 5) between 3.3 and 5 V in (A) $PYR_{14}TFSI$ and (B) $PYR_{14}FSI$. Insets: magnification of the high frequency part of the impedance.

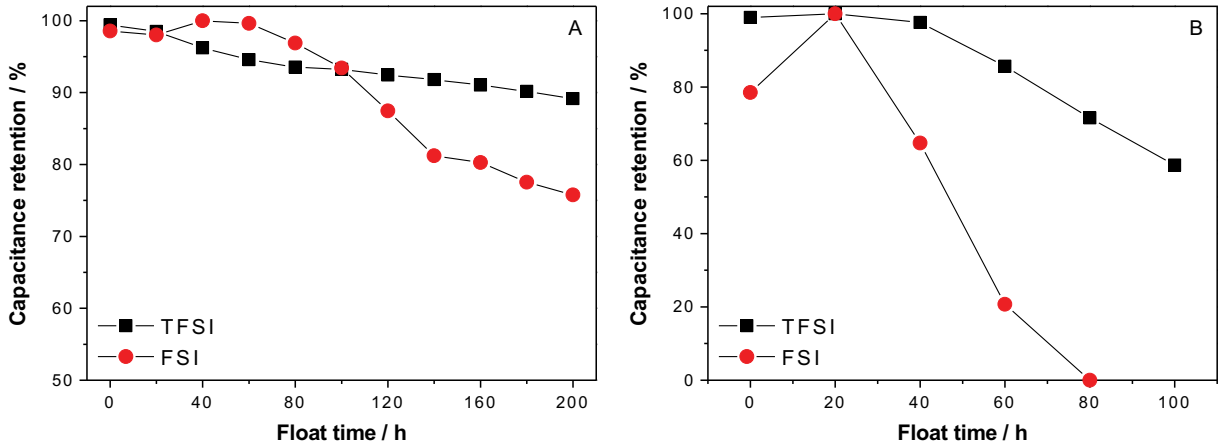

Fig. 7. Capacitance retention of EDLCs containing $PYR_{14}TFSI$ (TFSI) and $PYR_{14}FSI$ (FSI) as electrolyte, respectively, observed during float tests carried out at 3.5 V. The tests were carried out at (A) 20 °C and (B) 60 °C.

cycling efficiency already started to drop. The second broad semi-circle might be related to the formation of Al corrosion products that could clearly be found on the current collector after removal of the AC-based coating (Fig. 5C).

The abovementioned experiments give a clear indication about the different behavior of AC-based electrodes in $PYR_{14}FSI$ and $PYR_{14}TFSI$. Nevertheless, since they are referring to just one electrode, they cannot be considered as fully representative for the behavior of high voltage EDLCs. Therefore, EDLCs containing $PYR_{14}FSI$ and $PYR_{14}TFSI$ as electrolyte, respectively, were assembled and float tests at a cell voltage of 3.5 V were carried out at 20 and 60 °C (for details see Experimental section) (Fig. 7). Already at 20 °C, the capacitance of the cell based on $PYR_{14}FSI$ showed more pronounced fading than the one based on $PYR_{14}TFSI$ (Fig. 7A). After an activation phase during the first 60 h, the capacitance started to fade. Compared to $PYR_{14}TFSI$, the fading was more pronounced for the cell based on $PYR_{14}FSI$. After 200 h of polarization, the capacitance retention using $PYR_{14}FSI$ was *ca.* 75%, while it was *ca.* 90% when using $PYR_{14}TFSI$ as electrolyte. The stronger fading in the case of $PYR_{14}FSI$ can probably mostly be attributed to dissolution of the Al current collector and also to some electrolyte decomposition, while in the case of $PYR_{14}TFSI$ the capacitance fading was most likely only due to some electrolyte decomposition during the constant voltage steps at a cell voltage of 3.5 V.

At 60 °C, the differences in capacitance retention were even more pronounced (Fig. 7B). After 80 h, the $PYR_{14}FSI$-based cell could not store energy anymore; the capacitance was down to a value of zero. In contrast, the $PYR_{14}TFSI$-based cell could stand the higher temperature much better and showed capacitance retention of *ca.* 70% after 80 h. The very high capacitance fading in the case of $PYR_{14}FSI$ can mostly be attributed to electrolyte decomposition under these harsh conditions. Although the capacitance fading at 60 °C was also more pronounced when using $PYR_{14}TFSI$ as electrolyte than at 20 °C, it has to be pointed out that this electrolyte can most likely still be used for applications at 60 °C that do not require a constant state-of-charge of 100%. Furthermore, especially the capacitance retention under float conditions depends on the cell voltage. Slightly reducing the cell voltage will already lead to a marked improvement of the capacitance retention at 60 °C.

3.4. The influence of the chloride content of $PYR_{14}FSI$ on the cycling stability of high voltage EDLCs

So far, the question remained, why $PYR_{14}FSI$ showed a lower ability to prevent the corrosion of Al current collectors than $PYR_{14}TFSI$. From the XPS analysis (see above) no pronounced differences in the surface layer could be found. One explanation could be that the passivation layer in the case of $PYR_{14}FSI$ is less resistive to halide attack that can lead to the initialization of pitting corrosion. In order to investigate this point, we carefully prepared another batch of $PYR_{14}FSI$ with the aim to further reduce the level of halides. Ion chromatography showed that the chloride content of the second batch was <1 ppm. The chloride content of the first batch was >2 ppm. We then carried out the same float test at 20 °C as presented above. Fig. 8A shows the results obtained for $PYR_{14}TFSI$ and the two batches of $PYR_{14}FSI$. Interestingly, the capacitance retention using the batch of $PYR_{14}FSI$ with smaller chloride content was similar to the one for $PYR_{14}TFSI$. Also the change in impedance during 200 h of constant voltage was similar to the one measured for the $PYR_{14}TFSI$-based cell. The main difference was that the high frequency resistance slightly increased in the case of $PYR_{14}FSI$, indicating some electrolyte decomposition, while the one in the case of $PYR_{14}TFSI$ remained more constant. In contrast, the impedance of the cell employing the batch of $PYR_{14}FSI$ with higher chloride content changed more pronounced: A bigger semi-circle appeared and also the increase of the high frequency resistance was stronger, indicating a contribution of Al corrosion products to the cell resistance.

To verify the influence of the chloride content on the anodic stability of Al electrodes in $PYR_{14}FSI$, cyclic voltammetry up to 5 V was also carried out for the electrolyte with a chloride content of <1 ppm (Fig. 9A). The shape of the CV curves was similar to the ones obtained for $PYR_{14}TFSI$. No hysteresis occurred and the current density at 5 V continuously decreased over cycling. Only a broad peak at *ca.* 3.9 V slowly appeared over cycling. However, the current density of this peak remained below 1 μA cm^{-2}. It is unclear, whether this peak originated from the onset of a very mild Al corrosion process or from the oxidation of electrolyte decomposition products forming at high potentials. In the inset of Fig. 9A, the current densities of the last cycles obtained for both $PYR_{14}FSI$ electrolytes is presented. Obviously, the current densities were more than 10 times higher in the case of the electrolyte with >2 ppm of chloride. Furthermore, the current also remained high during the reverse scan. In contrast, when the chloride content of the electrolyte was <1 ppm, the current dropped when the scanning direction was reversed. The SEM image taken after the CV experiment in $PYR_{14}FSI$ with very low chloride content (Fig. 9B) was very similar to the one taken after the same experiment in $PYR_{14}TFSI$. No corrosion pits could be found on the surface of the electrode. This result confirms the excellent anodic stability of Al in

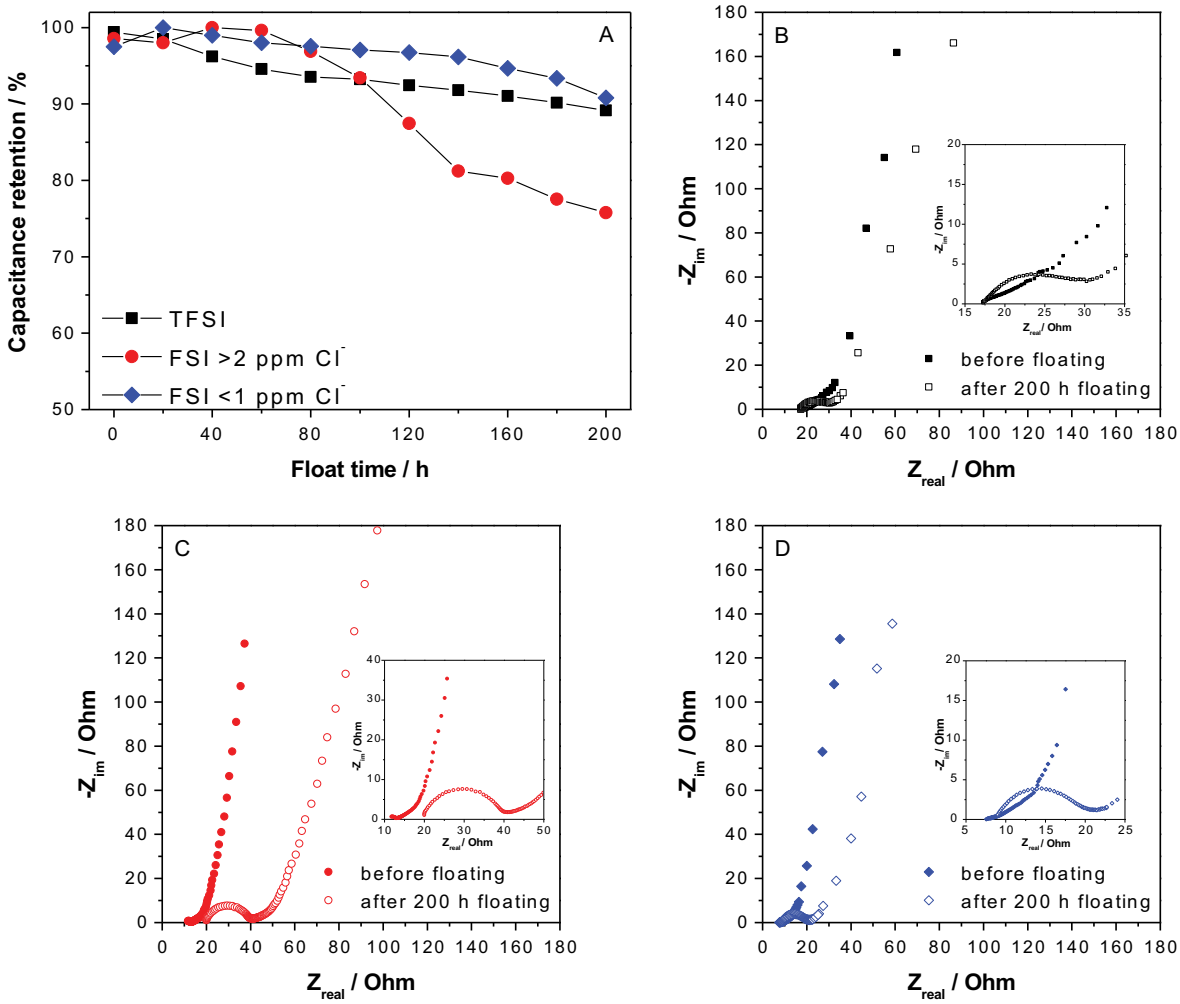

Fig. 8. (A) Capacitance retention of EDLCs containing $PYR_{14}TFSI$ (TFSI) and $PYR_{14}FSI$ with a chloride content of >2 ppm (FSI > 2 ppm Cl^-) and <1 ppm (FSI <1 ppm Cl^-) as electrolyte, respectively, observed during float tests carried out at 3.5 V. (B–D) Evolution of the impedance of the same EDLCs using (B) $PYR_{14}TFSI$ and using (C) $PYR_{14}FSI$ with a chloride content of >2 ppm and (D) <1 ppm as electrolyte. Insets: Magnification of the high frequency part of the impedance. The tests were carried out at 20 °C.

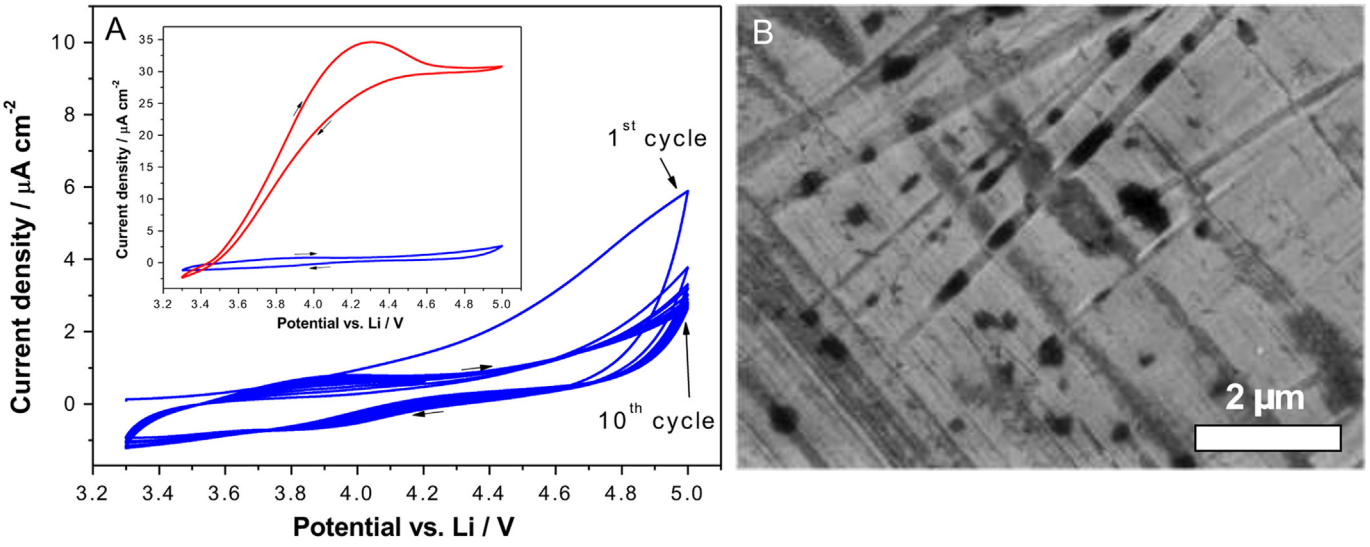

Fig. 9. (A) Cyclic voltammogram of an Al electrode recorded between 3.3 and 5 V vs. a lithium reference in $PYR_{14}FSI$ with a chloride content of <1 ppm at 20 °C. Scan rate: 0.5 mV s^{-1}. An activated carbon-based electrode was used as counter electrode. Inset: Comparison of the 10th cycles using $PYR_{14}FSI$ with a chloride content of >2 ppm (upper curve) and <1 ppm (lower curve) as electrolyte. (B) SEM image of the Al electrode taken after the CV experiment in the $PYR_{14}FSI$ electrolyte with a chloride content of <1 ppm.

high purity $PYR_{14}FSI$. It also indicates that the corrosion process found for $PYR_{14}FSI$ was indeed related to halide impurities and that careful control of the level of impurities leads to a good suppression of the corrosion process.

4. Conclusions

Supercapacitors employing FSI-based ionic liquids like $PYR_{14}FSI$ can more easily suffer from Al corrosion than the ones based on $PYR_{14}TFSI$. This effect is not easily detectable in tests typically run to investigate novel electrolytes for EDLCs because the corrosion process is much less pronounced than *e.g.* the one in PC–LiTFSI. Therefore, either slow cycling or float tests are needed to detect the Al dissolution in a reasonable time. Nevertheless, considering the typical $>10^6$ charge/discharge cycles rating of EDLCs, the detrimental effect on the long-term cycling stability of such devices cannot be neglected. For applications where the energy stored in the supercapacitor is released shortly after charging, the total time spent at high potentials might be short enough to prevent negative effects on the cycling stability due to Al corrosion for a quite high number of cycles. Finally, also the operative voltage and the temperature play a big role. The higher the average voltage excursion of the positive electrode, the faster will be the Al dissolution. At 60 °C, $PYR_{14}FSI$-based cells suffered from very fast capacitance fading during a float test at 3.5 V.

Interestingly, we found first evidence that the anodic stability of Al current collectors in $PYR_{14}FSI$ can be strongly improved by limiting the level of chloride impurities to values <1 ppm. In the future, the dependence of the anodic behavior of Al in FSI-based ILs on the level of halide impurities will be investigated in more detail.

Acknowledgments

The authors wish to thank the Westfälische Wilhelms-Universität Münster and the Ministerium für Innovation, Wissenschaft, Forschung und Technologie des Landes Nordrhein-Westfalen (MIWFT) for the financial support.

References

[1] M. Galiński, A. Lewandowski, I. Stępniak, Electrochim. Acta 51 (2006) 5567–5580.
[2] M. Ishikawa, T. Sugimoto, M. Kikuta, E. Ishiko, M. Kono, J. Power Sources 162 (2006) 658–662.
[3] P. Reale, A. Fernicola, B. Scrosati, J. Power Sources 194 (2009) 182–189.
[4] H. Matsumoto, H. Sakaebe, K. Tatsumi, M. Kikuta, E. Ishiko, M. Kono, J. Power Sources 160 (2006) 1308–1313.
[5] M. Egashira, A. Kanetomo, N. Yoshimoto, M. Morita, J. Power Sources 196 (2011) 6419–6424.
[6] J. Reiter, M. Nádherná, R. Dominko, J. Power Sources 205 (2012) 402–407.
[7] A. Balducci, R. Dugas, P.L. Taberna, P. Simon, D. Plée, M. Mastragostino, S. Passerini, J. Power Sources 165 (2007) 922–927.
[8] A. Lewandowski, A. Olejniczak, M. Galinski, I. Stepniak, J. Power Sources 195 (2010) 5814–5819.
[9] W.-Y. Tsai, R. Lin, S. Murali, L.L. Zhang, J.K. McDonough, R.S. Ruoff, P.-L. Taberna, Y. Gogotsi, P. Simon, Nano Energy 2 (2013) 403–411.
[10] C. Arbizzani, M. Biso, D. Cericola, M. Lazzari, F. Soavi, M. Mastragostino, J. Power Sources 185 (2008) 1575–1579.
[11] N. Handa, T. Sugimoto, M. Yamagata, M. Kikuta, M. Kono, M. Ishikawa, J. Power Sources 185 (2008) 1585–1588.
[12] G.B. Appetecchi, M. Montanino, A. Balducci, S.F. Lux, M. Winter, S. Passerini, J. Power Sources 192 (2009) 599–605.
[13] B. Garcia, M. Armand, J. Power Sources 132 (2004) 206–208.
[14] C. Peng, L. Yang, Z. Zhang, K. Tachibana, Y. Yang, J. Power Sources 173 (2007) 510–517.
[15] J. Mun, T. Yim, C.Y. Choi, J.H. Ryu, Y.G. Kim, S.M. Oh, Electrochem. Solid-State Lett. 13 (2010) A109–A111.
[16] E. Cho, J. Mun, O.B. Chae, O.M. Kwon, H.-T. Kim, J.H. Ryu, Y.G. Kim, S.M. Oh, Electrochem. Commun. 22 (2012) 1–3.
[17] R.-S. Kühnel, M. Lübke, M. Winter, S. Passerini, A. Balducci, J. Power Sources 214 (2012) 178–184.
[18] C. Peng, L. Yang, Z. Zhang, K. Tachibana, Y. Yang, S. Zhao, Electrochim. Acta 53 (2008) 4764–4772.
[19] X. Wang, E. Yasukawa, S. Mori, Electrochim. Acta 45 (2000) 2677–2684.
[20] G.B. Appetecchi, S. Scaccia, C. Tizzani, F. Alessandrini, S. Passerini, J. Electrochem. Soc. 153 (2006) A1685–A1691.
[21] R.-S. Kühnel, N. Böckenfeld, S. Passerini, M. Winter, A. Balducci, Electrochim. Acta 56 (2011) 4092–4099.
[22] Q. Zhou, W.A. Henderson, G.B. Appetecchi, M. Montanino, S. Passerini, J. Phys. Chem. B 112 (2008) 13577–13580.
[23] G.B. Appetecchi, M. Montanino, D. Zane, M. Carewska, F. Alessandrini, S. Passerini, Electrochim. Acta 54 (2009) 1325–1332.
[24] R. Lin, P.-L. Taberna, S. Fantini, V. Presser, C.R. Pérez, F. Malbosc, N.L. Rupesinghe, K.B.K. Teo, Y. Gogotsi, P. Simon, J. Phys. Chem. Lett. 2 (2011) 2396–2401.
[25] H. Yang, K. Kwon, T.M. Devine, J.W. Evans, J. Electrochem. Soc. 147 (2000) 4399–4407.
[26] S.-T. Myung, Y. Hitoshi, Y.-K. Sun, J. Mater. Chem. 21 (2011) 9891–9911.
[27] J.L. Allen, D.W. McOwen, S.A. Delp, E.T. Fox, J.S. Dickmann, S.-D. Han, Z.-B. Zhou, T.R. Jow, W.A. Henderson, J. Power Sources 237 (2013) 104–111.
[28] S.-T. Myung, Y. Sasaki, S. Sakurada, Y.-K. Sun, H. Yashiro, Electrochim. Acta 55 (2009) 288–297.
[29] M. Montanino, F. Alessandrini, S. Passerini, G.B. Appetecchi, Electrochim. Acta 96 (2013) 124–133.